Ultra-sensitive detection of individual gold nanoparticles: spectroscopy and applications to biology

Laurent Cognet and Brahim Lounis

Centre de Physique Moléculaire Optique et Hertzienne, Université de Bordeaux and CNRS, 351 cours de la libération, Talence, F-33405 France

Gold nanoparticles are now widely used in different fields of chemistry, physics and biology. For many applications, it became crucial to use the smallest ones and at the same time to be able to detect them at the single particle level with versatile optical methods. Such methods should also allow the study of their intimate optical properties. Here we review the ultra-sensitive optical methods based on the photothermal effect which permit the detection of individual gold nanoparticles down to 1.4 nm through their absorption. The absorption spectroscopy of the Surface Plasmon Resonance of individual gold nanoparticles down to 5nm is further presented and revealed intrinsic size effects in the optical response of the smallest nanoparticles. Different applications to biology are also presented such as for new types of gold nanoparticles based DNA microarrays and for live cell molecular imaging owing to the insensitivity of the photothermal methods to scattering environments.

Gold nanoparticles (AuNPs) exhibit fascinating physical properties, either taken as individuals or in assemblies. The remarkable behavior of the individual AuNPs comes from their size-related electronic and optical properties (1, 2), which has opened many applications in different fields such as in catalysis (3), plasmonics (4), biosensing (5) or biology (6, 7). For use of their full potential, sensitive methods which allow the detection and spectroscopy of individual small AuNPs are however needed. Indeed, selecting a single nano-object at a time allows the elimination of all the implicit averages of conventional optical observations (8), gaining access to heterogeneity (in size, shape or local environment), dynamical fluctuations, diffusion, reorientation, or colocalization at the molecular level. Yet, the optical detection of a single nano-object remains difficult, because the spatial resolution is limited by the wavelength of light, so that the signal must be extracted from the background arising from its environment in the focal spot of the microscope. In the past 20 years, researchers have used dark-field illumination (9), differential interference contrast and video enhancement (10), or total internal reflection (11) methods to optically detect metal nanoparticles through their Rayleigh intensity scattering (12, 13). However, such techniques are generally limited to the detection of relatively large particles (>40 nm) because the scattered intensity decreases sharply with the nano-object size and becomes swallowed up in the background from other scatterers (14). Consequently, new methodologies were needed to allow the detection of very small AuNPs in complex environments.

The polarizability of a AuNPs interacting with a laser field being proportional to its volume, intensity-scattering cross-section of the particle, varies as D^6, while its absorption cross-section varies as D^3 only. For AuNPs interacting with a 532-nm laser light in water, absorption dominates the optical response for nanoparticles diameters below 100 nm. In non-scattering environments, it was demonstrated that it is possible to detect directly the absorption of small nanoparticles (15). The use of the interference between a reference field and the field scattered by an nanoparticle to get a signal that, similarly to absorption varies with the third power of the particle size has also been proposed (16, 17). This interferometric techniques can give access to both the amplitude and the phase of the scattered wave. A recent review dedicated to scattering- and absorption-based schemes yielding a signal proportional to the third power of the nanoparticle size was published recently (14).

In the following, we will focus on the methods that are based on the photothermal effect -a consequence of absorption- and thus also provide signals varying with the third power of the particle size. To date, they are the most sensitive ones and present the advantage to be applicable in highly scattering environments. This makes them suitable for a broad range of fundamental and applied studies such as absorption spectroscopy of small nano-objects or live cell imaging. In the next sections we first introduce the principle of the photothermal detection methods, we then present the

absorption spectroscopy of tiny AuNPs and finally introduce some applications in biosciences.

Excited near their surface plasmon resonance (SPR), metal nanoparticles have a large absorption cross-section and exhibit a fast electron-phonon relaxation time in the picosecond range (18), which makes them very efficient light absorbers. The luminescence yield of these particles being extremely weak (19), almost all the absorbed energy is converted into heat. The increase of temperature induced by this absorption gives rise to a local variation of the refractive index. This photothermal effect can be used to detect and study AuNPs. Photothermal detection was proposed earlier by Tokeshi et al. (20), who used a thermal lens effect to detect very low concentrations of absorbing molecules in liquid solutions. Boyer et al. (21) designed a highly sensitive polarization interference method, called Photothermal Interference Contrast (PIC), for the detection of the small refractive index changes around an absorbing particle. The experiment was performed using a combination of two lasers. The nanoparticles were heated by the 514-nm line of an argon ion laser, which intensity was modulated at high frequency. The horizontally polarized output of a He-Ne laser (633 nm wavelength) was split into two perpendicularly polarized beams by a Wollaston prism forming the two arms of the interferometer (probe and reference). The probe beam was overlaid with the heating beam, and the different beams were sent to a microscope objective using a telecentric lens system. The probe and reference beams back-reflected by the sample recombined in the Wollaston prism and were reflected by a polarizing beamsplitter cube onto a fast photodiode (Figure 1a). A lock-in amplifier detected the variations of the red intensity and thus the phase difference between the two red beams at the modulation frequency of the green beam. Microscopic images were obtained by scanning the sample with respect to the three spots. With PIC, images of AuNPs down to 5 nm in diameter embedded in thin polymer films were recorded with a signal-to-noise ratio larger than 10 (Figure 1b). The authors also showed that, in addition to their intrinsic sensitivity, the photothermal method is remarkably insensitive to scattering background, even when arising from strong scatterers such as 300-nm latex beads. The sensitivity of the PIC method, although high, could not reach the shot noise limit. Indeed, the use of high numerical-aperture objectives induced depolarization effects which degraded the quality of the overlap between the two arms of the interferometer. As a consequence, the detection of nanometer sized particles with PIC required relatively high laser intensities (~10 MW/cm^2), which can be a serious limitation for many applications such as in biology.

Berciaud et al. then developed a more sensitive photothermal method, called Photothermal Heterodyne Imaging (PHI) (22, 23) (alternatively called "Laser Induced Scattering Around a NanoAbsorber", LISNA for biological applications (24, 25)). It combines a time-modulated heating beam and a non-resonant probe beam, overlapping on the sample. When a small AuNPs is illuminated by the intensity modulated heating beam (modulation frequency Ω), it behaves like a heat point source and generates a time-modulated index of refraction in its vicinity. The probe beam interacting with this profile gives rise to a scattered field containing sidebands with frequency shifts at Ω. As in any heterodyne technique, interference between a reference field (either the reflection of the incident probe at the interface between a cover slip and the sample or its transmission, see Figure 2(a)) and the scattered field produces a beatnote at the modulation frequency Ω which can be easily extracted with a lock-in amplifier.

In practice, a non resonant probe beam (632.8 nm, HeNe, or single frequency Ti:Sa laser) and an absorbed heating beam (532 nm, frequency doubled Nd:YAG laser or tunable cw dye laser) are overlaid and focused on the sample by means of a high NA microscope objective (100x, NA=1.4). The intensity of the heating beam is modulated at Ω ranging from typ. 100kHz to a few MHz, by an acousto-optic modulator. The PHI signal can be detected using two different configurations. In the case of the detection of the backward signal, a combination of a polarizing cube and a quarter wave plate is used to extract the interfering probe-reflected and backward-scattered fields. In order to detect the forward signal, a second microscope objective (80x,

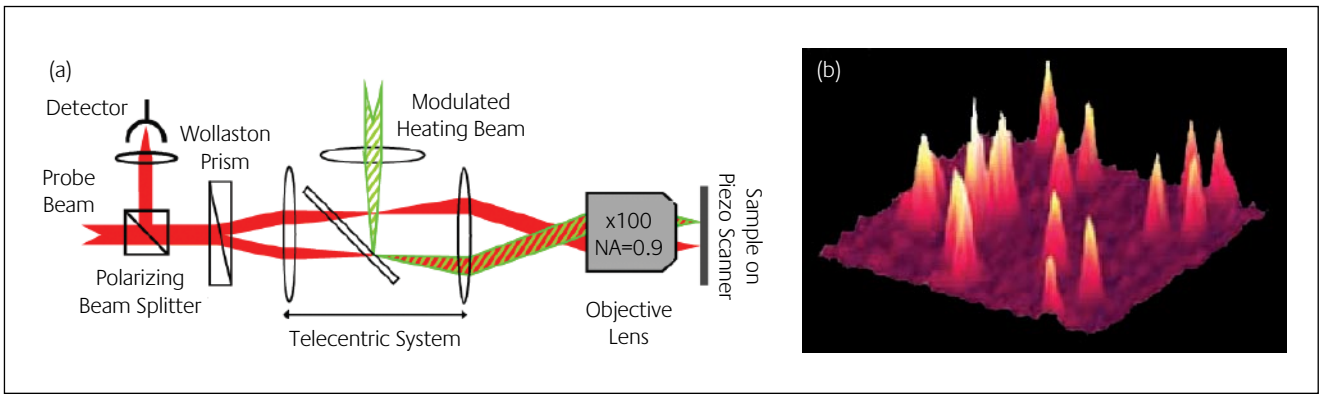

Figure 1

a) Experimental scheme of the Photothermal interference contrast (PIC) method. b) PIC image of a 10x10μm^2 region of sample containing isolated 5nm AuNPs

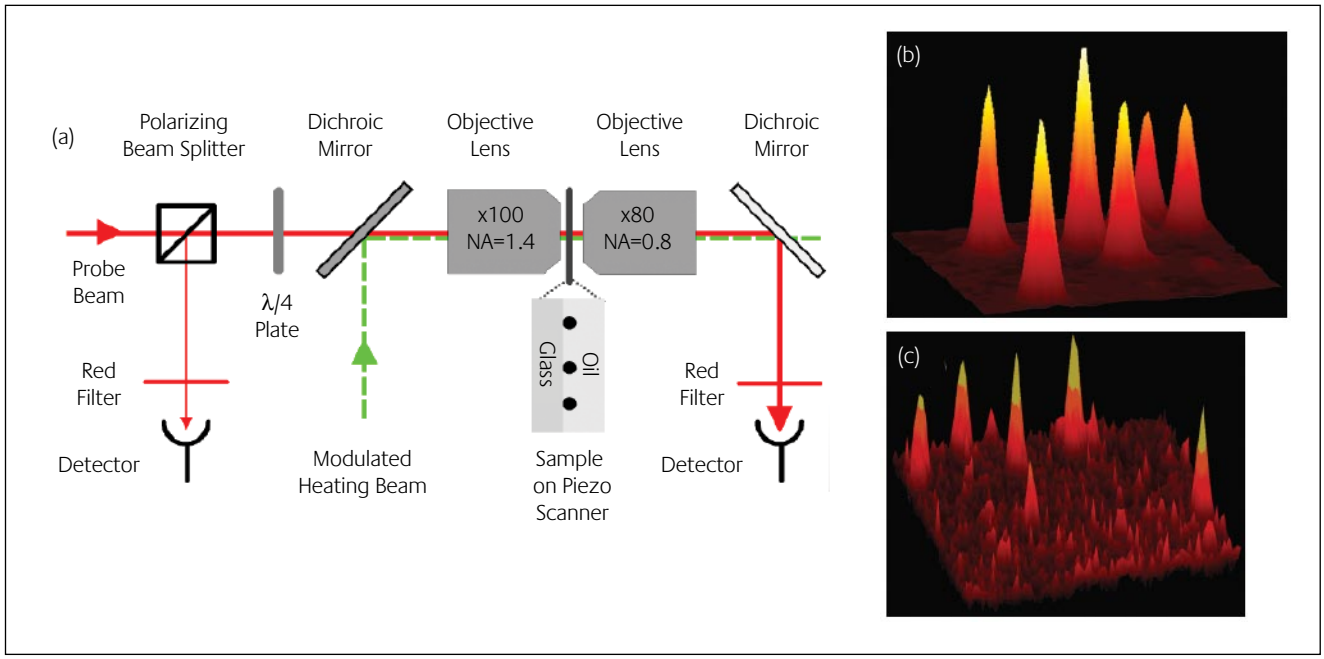

Figure 2

a) Experimental scheme of the Photothermal heterodyne imaging (PHI) method. The backward configuration uses the left detector, while the forward uses the right one. b) PHI image of a 6x6μm² region of sample containing isolated 5nm AuNPs. c) PHI image of a 5x5μm² region of sample containing isolated 1.4nm AuNPs

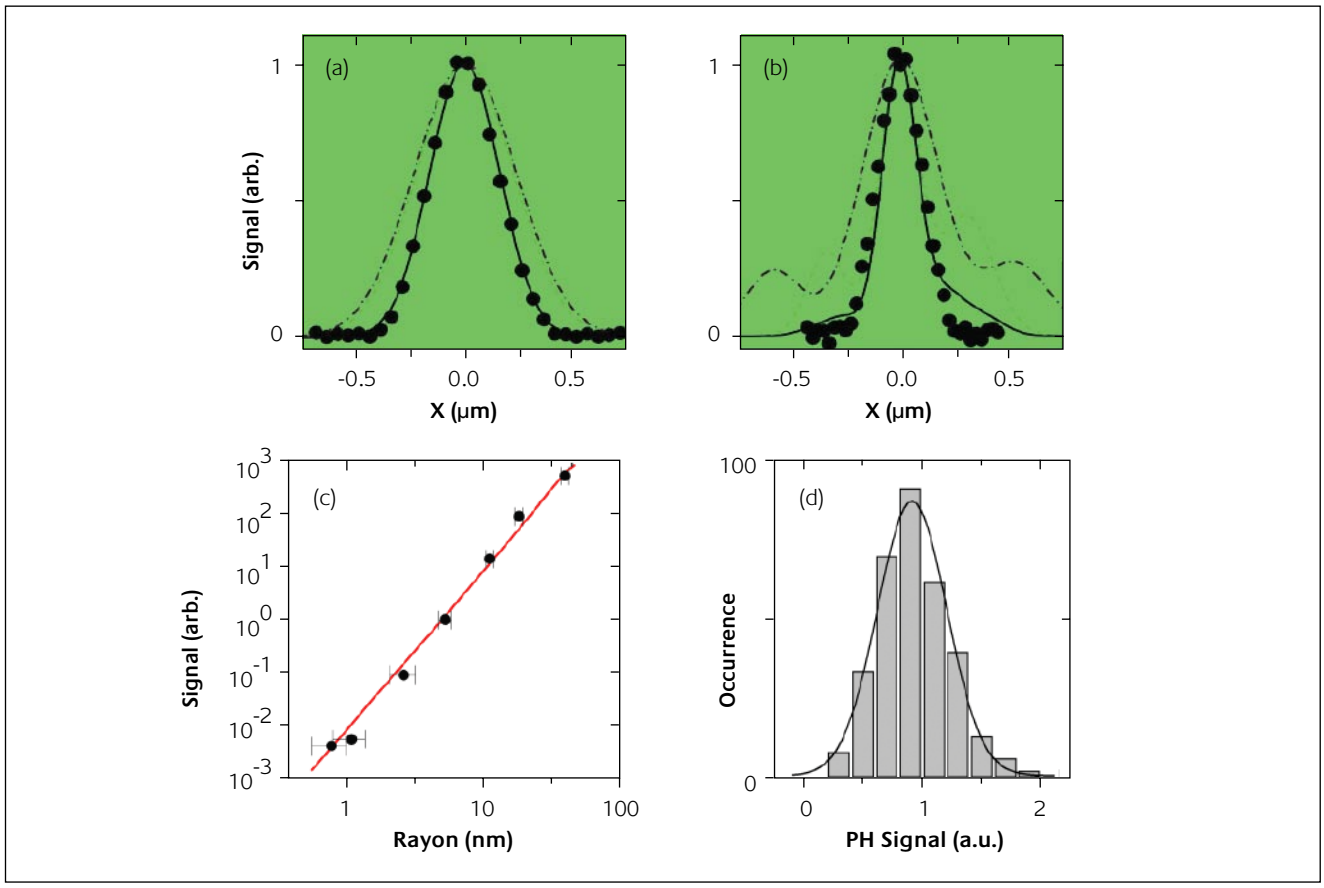

Figure 3

Transverse resolution of the PHI method with low (a) and high (b) aperture of the beams. The measured profiles of the probe beam (red, dashed-dotted lines) and heating beam (green, dashed lines) are indicated. In both cases, the profile of the PHI signal from a single 10nm gold NP (circles) is in very good agreement with the product of the two beams profiles (solid line). The transverse resolutions of the PHI signals are (a) 365 ±5 nm (FWHM) and (b) 235±5 nm (FWHM). (c) Size dependence of the signal i.e. absorption cross section (circles) deduced from samples containing different sizes of AuNPs and comparison to the Mie theory (solid line) (d) Signal histogram of 321 peaks detected in a sample prepared with 10nm gold NPs with a dispersion in diameter of 10%. The monomodal shape of the distribution reveals that individual NPs are detected

NA=0.8) is employed to efficiently collect the interfering probe-transmitted and forward-scattered fields. The intensity of the heating beam sent on the AuNPs ranges from less than $1 kW/cm^2$ to ~$5 MW/cm^2$ (depending on the desired signal-to-noise ratio and the NP size to be imaged). Backward or forward interfering fields are collected on fast photodiodes and fed into a lock-in amplifier in order to extract the beat signal at Ω. Integration time of 10 ms are typically used. Images are formed by moving the sample over the fixed laser spots by means of a 2D piezo-scanner. PHI can be shot-noise limited since it does not suffer from the limitations inherent to PIC. Its sensitivity is more than one order of magnitude higher than that of any other method (Figure 2b). This sensitivity enabled the unprecedented detection of individual gold clusters as small as 1.4 nm in diameter, which contain less than 100 atoms (Figure 2c).

The resolution of the PHI method depends on the probe and heating beam profiles and also on the dielectric susceptibility profile created around the AuNPs. Since the spatial extension of the latter is much smaller than the size of the probe beam, the transverse resolution is simply given by the product of the two beams profiles (Figure 3a-b).

The PHI signal is proportional to the absorption cross-section of the nanoparticles. It thus scales with the volume for small size particles excited at given heating wavelength (Figure 3c). Therefore, the dispersion in signals obtained from image of a sample containing individual AuNPs with size dispersion of 10% will be equal to 30% around a mean signal as exemplified on Figure3d. The unimodal distribution of the signal values and its dispersion confirm that individual AuNPs are imaged.

Absorption spectroscopy of individual gold nanoparticles

Noble metal nanoparticles are strong absorbers and scatterers around their SPR which falls in the visible range. The corresponding resonant peak energies and line-widths are sensitive to the nanoparticle size, shape and nano-environment(1).

The spectral properties of the SPR have been extensively studied on ensembles of noble NPs and compared to Mie theory (26, 27). For rather large nanoparticles (diameter D ≥ 20nm), the resonant peak energy E_R experiences a red-shift with increasing sizes, due to retardation effects as well as to increasing contributions from multipolar terms. In addition, for AuNPs larger than 50 nm, radiative damping of the collective electronic excitation significantly broadens the linewidth of the SPR (26, 27). For smaller NPs (D < 20 nm), these extrinsic size-effects become negligible and intrinsic size-effects prevail. They account for size-dependent modifications of the dielectric constant with respect to the bulk values, due to additional surface damping (1, 28) and translate into a broadening of SPR linewidths with decreasing sizes, and to a lower extent, into slight shifts of E_R. Comparisons between theory and ensemble measurements are still a matter of debate because the inhomogeneities in nanoparticle size, shape and local environment experimentally hide the homogenous width of the SPR.

For large AuNPs (NPs with D ≥ 20 nm), scattering-based methods previously allowed to perform SPR spectroscopy on individual particles and to study the extrinsic size-effects (11, 29). No intrinsic-size effects due to additional surface

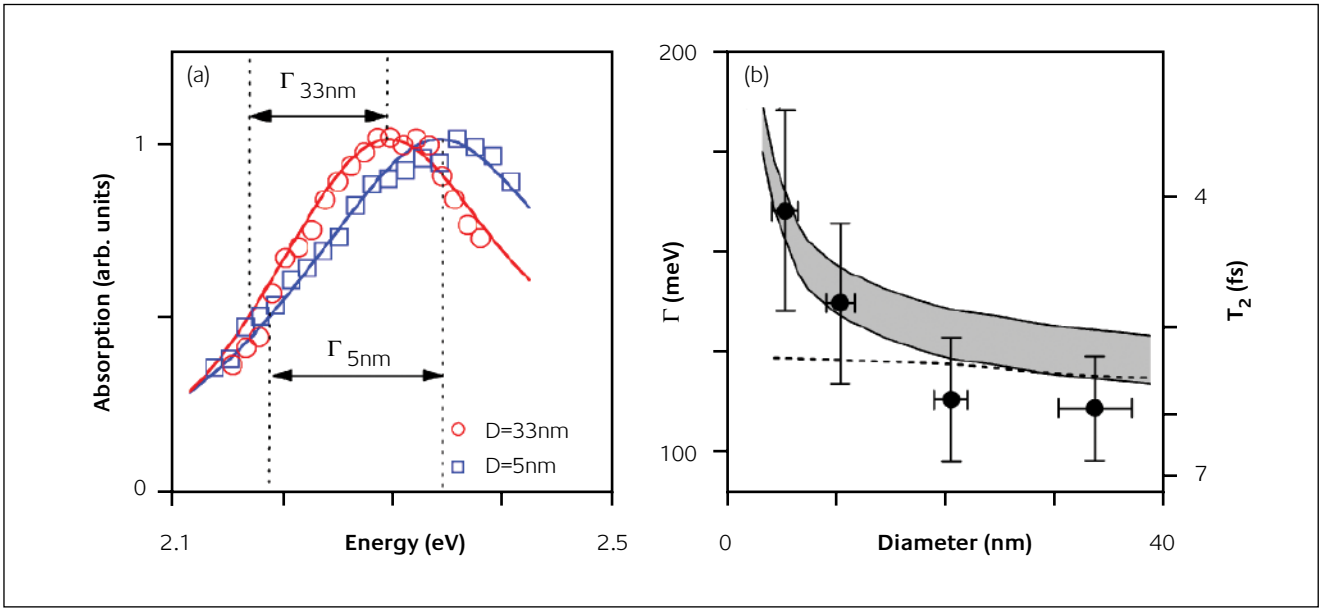

Figure 4

a) Normalized absorption spectra of 2 single AuNPs of diameters 33 nm (open circles) and 5 nm (open squares). The extracted width at half-maximum is shown on both nanoparticle spectra. The experimental spectra are compared with simulations based on Mie theory (solid lines) using a size-dependent modification in the dielectric constant of gold. (b): Size-dependence of the plasmon resonance width. Experimental data (circles with standard deviations) are compared with Mie theory without (dotted line) and with (gray area) size dependent correction

damping were observed since a good agreement was found with Mie theory using the bulk values for the metal dielectric function (30).

Berciaud et al took advantage of the high sensitivity of PHI to study for the first time the absorption spectra of individual AuNPs with diameter down to 5 nm (31). For this purpose a cw linearly polarized dye laser was used as heating beam. Wavelength-dependent angular deviations were compensated by double pass through the acousto-optic modulator. In order to avoid any dependence of the relaxation dynamics of electrons on the absorbed power, the experiments were performed in the weak excitation regime where the average time between two successive absorption events is significantly longer than the relaxation times in AuNPs (18). This corresponds to heating powers ranging from ≈ *1 μW* to ≈ *500 μW* (for *D* = *33 nm* to D = *5 nm* respectively), allowing to image the individual NPs with signal-to-noise ratios greater than 10 at the peak resonant energies for 10ms integration times. Prior to spectra acquisitions, single AuNPs were first located by imaging a 10x10 μm^2 area of the sample at fixed heating wavelength. For each single AuNPs, spectra were then acquired by automatically sweeping the laser photon energy by steps of 10 meV across the resonance with a 2 s integration time per point. The photothermal signals were corrected for the wavelength dependence of the diffraction-limited laser spot size. The heating power was measured during the acquisitions and used to normalize the spectra.

Figure 4a shows examples of absorption spectra recorded for 2 individual AuNPs (*D* = 5 and 33nm). One can already notice that both a blue-shift and a broadening of the SPR with decreasing particle sizes are clearly visible. The SPR spectra are asymmetric due to interband transitions. Indeed, in gold, the energy threshold for interband transitions lies at ~2.4 eV and is preceded by an absorption tail starting at about 1.8 eV (32). Defining a full-width-at-half maximum of absorption spectra for AuNPs would thus be delicate, and even impossible for very small particles. Instead, from each spectrum one can extract the peak resonant energy E_R, and the homogenous red half-width at half maximum Γ_D=E_R-$E_{1/2}$ where $E_{1/2}$ is the photon energy for which the absorption is half of the peak value.

For each AuNPs size *D*, Berciaud et al recorded about 30 spectra and extracted the mean values of E_R and Γ_D as well as their respective dispersions. The red-shift experienced by E_R for increasing sizes could be well reproduced by the theory using the bulk dielectric function of gold (32). In contrast, Mie theory with the bulk dielectric functions only predicts a minor dependence of the SPR linewidth with particle size (dashed line in Figure 4b). In order to explain the experimental variations of Γ_D with *D*, surface effects have to be considered through a size-dependent dielectric function(1):

$$\varepsilon(\omega,D)=\varepsilon_{IB}(\omega)+1-\frac{\Omega_p^2}{\omega^2+i\omega\gamma(D)}$$

where Ω_p is the bulk plasma frequency. $\varepsilon(\omega,D)$ contains two contributions: the first, $\varepsilon_{IB}(\omega)$, is due to interband transitions and assumed to be size independent, whereas the second is the Drude-Sommerfeld free electron term. It contains the size-dependent phenomenological damping constant:

$$\gamma(D)=\gamma_0+2\frac{Av_F}{D}$$

where γ_0 is the bulk damping rate and v_f is the Fermi velocity of the electrons. For gold, $h\Omega_p$=9.0 eV, $h\gamma_0$≈70 *meV* and v_f = 1.4 *nm fs*$^{-1}$. The dimensionless size parameter A accounts for additional surface damping terms. More precisely, surface scattering is usually described in terms of inelastic collisions which shorten the electron mean free path when the AuNPs sizes decrease. Additionally, for embedded AuNPs, chemical interface damping, i.e. fast energy transfer between the AuNPs and its close surrounding, may also damp the phase coherence of the collective oscillation (1, 33) when the particle plasmon energy is close to adsorbate energy levels. As the number of conduction electrons participating in the collective oscillation is proportional to the volume of the AuNPs, the size dependent correction in $\gamma(D)$ scales as the surface-to-volume ratio i.e. $\frac{1}{D}$.

Using the Mie theory with the size-dependent dielectric function, the absorption spectra for the different particles sizes was simulated and A=0.25 was found to be the best value for the size parameter to reproduce the experimental values of Γ_D. One should mention that Γ_D contains the two damping contributions mentioned above. Interestingly, the introduction of the non-zero value of A does not significantly

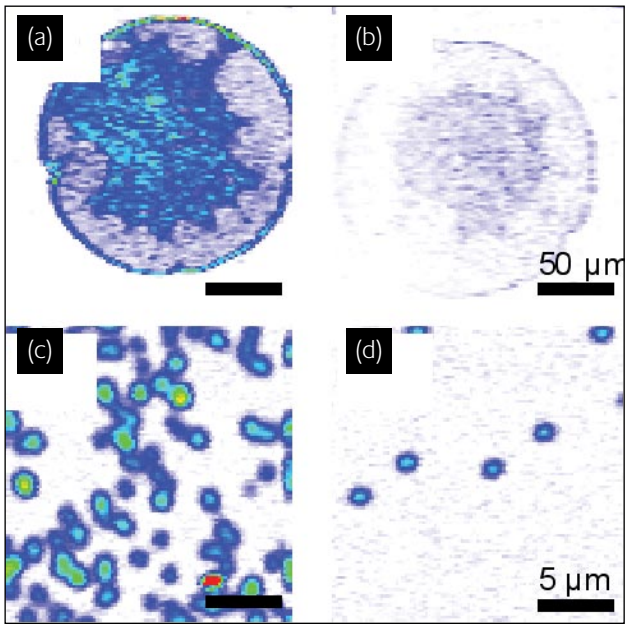

Figure 5

(a, b) Direct imaging (no silver enhancement) of 2 spots of a micro-array by PHI at low resolution (200x200μm^2, 2μm per point). The spots contained an average of 300 (a) and 20 (b) AuNPs/100μm^2 respectively. (c, d) Increasing the resolution (20x20μm^2, 200nm per point) allows individual AuNPs to be resolved. The spots imaged contained an average of 20 (c) and 2 (d) AuNPs /100μm^2 respectively

affect the expected values of E_R which maintains the agreement between the measurements and Mie simulations. In conclusion, the non zero value of *A*, is a clear signature of the presence of intrinsic size effects in the absorption spectra of small AuNPs, below 10nm.

Although the existence of intrinsic size effects in the optical response of AuNPs was unambiguously revealed, part of the damping processes are due to interband transition, which makes it difficult to connect the widths of the SPRs to the damping rate. A way to circumvent this additional damping would consist in red-shifting resonant energies towards photon energy smaller than the onset of interband transition. This can be done either by embedding spherical gold NPs in a matrix with high refractive index or by studying the SPR of the long axis mode in gold nanorods (30, 34) or even by using core-shell AuNP(35) which are actively studied for applications in biology (7).

Another possibility consists in using spherical silver NPs instead of AuNPs (13). Indeed for silver, the resonant energy of spherical NPs embedded in a medium with refractive index n=1.5 is at ~3 eV, whereas interband transitions start at ~3.7 eV (32). Contrary to gold, the SPR width of silver NPs has no contribution from interband transitions and it corresponds directly to the electron damping rate. Thus silver NPs are well adapted for studying the size dependence of ultrafast dephasing of the SPR at the single particle level. A limitation of silver NP is their weak photostability due to photo-oxydation (36). This limitation can be surpassed by using encapsulated silver NPs (37) e.g. with PEG (poly(ethylene glycol)) (38). Berciaud et al. (13) demonstrated the detection of individual PEG-coated silver nanoparticles with an average diameter of 5.3 nm with PHI microscopy. For these experiments, a modulated diode laser emitting at 405 nm was used as heating source with an intensity of ~50 kW/cm^2. As expected, the signal obtained with silver particles of 5.3 nm in diameter is about 10 times higher than that of AuNPs of the same size, when identical heating intensities are used to excite the nanoparticles at the peak of their SPR. The size distribution, however, was broad. Expected progress in the synthesis of silver nanoparticles with narrower size distributions should permit a quantitative study of the surface plasmon resonance of individual silver particles much smaller than 5 nm in diameter.

The high sensitivity provided by PHI, coupled to a better control of the NPs synthesis should allow original studies of light-nanoparticle interaction processes and we foresee diverse applications in different fields such as in plasmonics or bioimaging.

Applications to biosciences

In a first demonstration, Blab et al. (39) showed that PHI could provide a new readout strategy of DNA micro-arrays based on AuNPs. The determination and exact quantification of gene expression is becoming increasingly important in basic

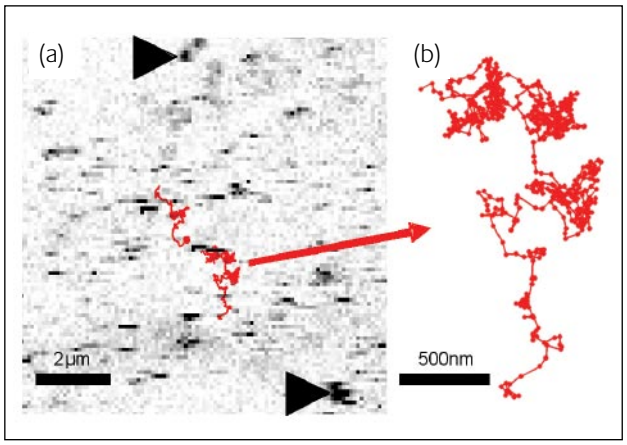

Figure 6

PHI image (a) of the portion of a live COS7 cell labelled with AuNPs. The image exhibits signals from moving (stripes) and stationary (arrows) membrane receptors labelled with AuNPs. Two trajectories of individual receptors labelled with 5nm AuNP (>1000 data points) acquired at video rate are shown in red. (b), Zoom on the bottom trajectory

pharmaceutical and clinical research. Fluorescence-based DNA assays are most widely used, but suffer from the presence of autofluorescence in some biological samples and substrates, which severely interferes with the detection of the target molecules. DNA assays based on AuNPs labels present a viable alternative. They commonly use AuNPs larger than 40 nm, which can be readily detected due to their strong light scattering at visible wavelengths (12, 13). For increased specificity and reactivity, AuNPs smaller than 40 nm are preferred. Indeed, small AuNPs functionalized with oligonucleotides exhibit a very sharp thermal denaturation profile, and the rate of reaction on a surface is much higher than with large particles (40-42). As small AuNPs (diameter, < 40 nm) barely interact with light, their direct optical detection has been impossible until recently without silver staining enhancement techniques (40, 42). However, saturation at the amplification step limits the linear dynamic range as the typical size of the silver crystals is much larger than that of the AuNPs (41). Furthermore, spontaneous conversion of silver solution into metallic grains can occur leading to nonspecific signals (41). Another alternative is the electrical detection of the AuNPs after catalytic or enzymatic deposition of the silver (43, 44). In this context, the possibility of detecting tiny AuNPs at the single particle level holds great promise for new and more efficient optical readout schemes of DNA assays.

PHI was thus applied on standard low-density spotted DNA microarrays in order to avoid the use of silver enhancement techniques. These arrays are well suited for routine applications as they contain a limited number of genes (usually below 1000), which enables good spotting quality and good reproducibility (45). PHI provided a reliable quantification of the amount of DNA molecules in each spot of the microarrays (39). This determination was no longer limited by any constraints of the detection method, but only by the degree of unspecific signals and by the size of

the AuNPs. Indeed, as all AuNPs are detected (Figure 5), the lower detection of DNA only depends on unspecific DNA hybridization events and on the quality of surface treatments. Concerning the upper detection limit, the ultimate limit is given by the condition of weak plasmon coupling between particles. Indeed, when the average distance of the small AuNPs is comparable to their size, the optical response of AuNPs is modified (46). Furthermore, the possibility to detect much smaller AuNPs (down to 1.4 nm) should significantly increase the dynamic range.

In addition to the high sensitivity and dynamics afforded by the present method, AuNPs-based DNA arrays can be stored and measured several times. This approach thus combines the advantages of fluorescence measurements -small marker size, purely optical detection- with the high stability, specificity, and dynamic range afforded by AuNP labelling techniques. This makes photothermal approaches promising for application in biochips.

Tiny AuNPs can also find applications when used as biomolecular labels for live cell imaging, in particular for the study of membrane proteins. The movements of molecules in the plasma membrane of living cells are characterized by their diversities, both in the temporal and spatial domain. Membranes exhibit a constitutive complexity, consisting of several different lipids and a great variety of proteins with highly dynamic and compartmentalized spatial distributions. These molecules explore the plasma membrane in various lateral diffusion modes, and frequently interact with another at specific locations in order to transmit information across the membrane, starting the cascades of specific signaling processes. Those molecular interactions are by nature heterogeneous making ensemble observations of these phenomena rather challenging. Single molecule detection has allowed the elimination of the implicit averaging of conventional optical observations. Until now, two main approaches have been used to track individual molecules in the plasma membrane of live cells, with distinct advantages and limitations. The first one, Single Particle Tracking (SPT), uses labels large enough to be detectable by conventional microscopes (47) through Rayleigh intensity scattering (~40 nm gold particles or even larger latex beads). SPT permits to follow the movement of individual molecules for very long times and possibly at very fast imaging rates (48). SPT, for instance, revealed barriers set for diffusion by the cytoskeleton (49), and the diversity of lateral diffusion modes of receptor for neurotransmitters in live neurons (50). However the main drawback is the size of the beads which might sterically hinder the interaction between the labelled molecules or alter their movements in confined environments such as synaptic clefts or endocytotic vesicles. The second widely used technique, Single Molecule Tracking (SMT), uses fluorescent organic dyes or autofluorescent proteins. As these fluorophores are generally smaller than the target molecules it does not have the drawback of SPT mentioned previously. Applied to neurosciences, SMT has thus allowed to reveal the lateral diffusion of glutamate receptors inside the synapses of live neurons (51). The main limitation encountered in SMT studies is photobleaching which severely limits the observation times of a single fluorophore to typically less than one second in live cells.

An experimental technique combining the advantages of SPT and SMT, namely long observation times and small nanometer-sized labels, would thus have great potential. For biological questions, it would allow for recording the full history of proteins in cells including intermediate states even in highly confined regions (e.g. lipid rafts or membrane protein clusters, intracellular vesicles, synapses of neurons....).

The advantages of the photothermal methods over fluorescent methods for single molecule detection were first demonstrated using PIC. Cognet et al. (52) could detect single proteins labelled with individual 10-nm AuNPs at the surface of fixed cells and showed the absence of saturation of the signals arising from the gold colloids, the insensitivity of the signal to the autofluorescence or scattering due to the environment - or to the cells themselves- and the absence of blinking and photobleaching of the labels. The latter limitation is very restrictive to perform 3D localization of the single fluorescent molecules as multiple records of the same molecule are hardly feasible. On the contrary, the stability of the PIC signals provided a way to localize in 3D single particles with a number of recordings and signal levels which can be arbitrary high. Single AuNPs could thus be localized in the scattering environment formed by a cell with very high pointing accuracy. As already mentioned, for live biological samples, the SNRs of the PIC method was however limited by the admissible temperature rise in the sample. For 10 nm AuNPs detected on the cell membranes with a SNR of 10, a temperature increase of 15K on the surface was estimated (52).

Later, PHI appeared as the method of choice for live cell imaging of very small metal nanoparticles (< 5 nm) with intensities compatible with cell integrity. An image of the portion of live COS7 cells with a low density of 5-nm-gold-labelled membrane receptors (mGluR5) on its outer membrane is presented in Figure 6a. As the PHI method requires a raster scan of the sample with typically a few-millisecond integration time per point, fast imaging rates cannot be readily obtained and moving objects are not resolved during the raster scan. Consequently, mobile receptors produce stripes of signal in the image whereas immobile ones can be resolved. Lasne et al. (25) designed a tracking scheme (SNaPT) based on a triangulation from three measurement points to record the trajectories of single membrane proteins labelled with AuNPs in live cells at video rate. The movement of single membrane receptors could thus be recorded for several minutes (Figure 6a and b). Single AuNP tracking combines the advantages of small marker size with practically unlimited observation times owing to the high chemical stability of gold particles. To estimate the local temperature rise due to laser absorption in the vicinity of the AuNPs, one can consider that the temperature inside a spherical AuNP is uniform and equal to the temperature at its surface since the thermal conductivity of metals is much

higher than that of the surrounding medium. It writes:

$$T_{surf} = \frac{\sigma_{abs} I}{4\pi\kappa a}$$

where I is the heating intensity, σ_{abs} the AuNP absorption cross section, κ the thermal conductivity of the medium (water) and a the radius of the AuNPs. For 5 nm AuNPs in aqueous medium, and I = 400 kW/cm^2 one finds a rather low AuNPs temperature rise of ~1.5 K. Furthermore it decreases as the inverse of the distance from the AuNPs surface.

Further improvements of the SNaPT method should allow not only studying 2D movements of single molecules on cultured cells but also 3D movements in more complex systems such as tissues slices. For instance, the algorithm used in SNaPT can be easily generalised for tracking movements of nanoparticles in 3D and we foresee that the use of near infrared excitation of small metal nanoparticles or nanorods would be advantageous to access deeper in the tissues.

Acknowledgements

This research was supported by CNRS (ACI Nanoscience and DRAB), ANR (PNANO program), Région Aquitaine, French Ministry for Education and Research (MENRT) and Human Frontiers Science Program (HFSP).

References

1 U. Kreibig, M. Vollmer, *Optical properties of metal clusters*, Springer-Verlag: Berlin, 1995
2 S. Eustis, M.A. El-Sayed, *Chemical Society Reviews*, 2006, **35**, 3, 209-217
3 M.C. Daniel, D. Astruc, *Chem. Rev.*, 2004, **104**, 1, 293-346
4 E. Ozbay, *Science*, 2006, **311**, 5758, 189-193
5 N.L. Rosi, C.A. Mirkin, *Chem. Rev.*, 2005, **105**, 4, 1547-1562
6 D.A. Schultz, *Current Opinion in Biotechnology*, 2003, **14**, 1, 13-22
7 L. Hirsch, A. Gobin, A. Lowery, F. Tam, R. Drezek, N. Halas, J. West, *Annals of Biomedical Engineering*, 2006, **34**, 1, 15
8 W.E. Moerner, M. Orrit, *Science*, 1999, **283**, 5408, 1670-1676
9 J. Yguerabide, E.E. Yguerabide, *J Cell Biochem Suppl*, 2001, **Suppl 37**, 71-81
10 M. Debrabander, R. Nuydens, G. Geuens, M. Moeremans, J. Demey, *Cell Motility And The Cytoskeleton*, 1986, **6**, 2, 105-113
11 C. Sönnichsen, S. Geier, N.E. Hecker, G. Von Plessen, J. Feldmann, H. Ditlbacher, B. Lamprecht, J.R. Krenn, F.R. Aussenegg, V.Z.H. Chan, J.P. Spatz, M. *Mo?Ller*, *Applied Physics Letters*, 2000, **77**, 19, 2949
12 J. Yguerabide, E.E. Yguerabide, *Anal Biochem*, 1998, 262, 2, 137-156
13 S. Schultz, D.R. Smith, J. J. Mock, D.A. Schultz, *Proc Natl Acad Sci USA*, 2000, **97**, 3, 996-1001
14 M.A. Van Dijk, A.L. Tchebotareva, M. Orrit, M. Lippitz, S. Berciaud, D. Lasne, L. Cognet, B. Lounis, *Physical Chemistry Chemical Physics*, 2006, **8**, 30, 3486
15 A. Arbouet, D. Christofilos, N. Del Fatti, F. Vallee, J.R. Huntzinger, L. Arnaud, P. Billaud, M. Broyer, *Phys Rev Lett*, 2004, **93**, 12, 127401
16 K. Lindfors, T. Kalkbrenner, P. Stoller, V. Sandoghdar, *Phys Rev Lett*, 2004, **93**, 3, 037401
17 F.V. Ignatovich, L. Novotny, *Physical Review Letters*, 2006, **96**, 1
18 S. Link, M.A. El-Sayed, *Annu Rev Phys Chem*, 2003, **54**, 331-366
19 J.P. Wilcoxon, J.E. Martin, F. Parsapour, B. Wiedenman, D.F. Kelley, *J Chem. Phys.*, 1998, **108**, 21, 9137-9143
20 M. Tokeshi, M. Uchida, A. Hibara, T. Sawada, T. Kitamori, *Analytical Chemistry*, 2001, **73**, 9, 2112
21 D. Boyer, P. Tamarat, A. Maali, B. Lounis, M. Orrit, *Science*, 2002, **297**, 5584, 1160-1163
22 S. Berciaud, L. Cognet, G.A. Blab, B. Lounis, *Phys. Rev. Lett.*, 2004, **93**, 25, 257402
23 S. Berciaud, D. Lasne, G.A. Blab, L. Cognet, B. Lounis, *Phys. Rev. B*, 2006, **73**, 045424
24 G.A. Blab, L. Cognet, S. Berciaud, I. Alexandre, D. Husar, J. Remacle, B. Lounis, *Biophysical Journal*, 2006, **90**, 1
25 D. Lasne, G.A. Blab, S. Berciaud, M. Heine, L. Groc, D. Choquet, L. Cognet, B. Lounis, *Biophysical Journal*, 2006, **91**, 12, 4598
26 G. Mie, *Ann. Phys.*, 1908, **330**, 377–445
27 C.F. Bohren, D.R. Huffman, J. Wiley (New York), 1983
28 S. Link, M.A. El Sayed, *Int. Reviews in Physical Chemistry*, 2000, **3**, 19, 409-453
29 J.J. Mock, M. Barbic, D.R. Smith, D.A. Schultz, S. Schultz, *J. Chem. Phys.*, 2002, **116**, 6755.
30 C. Sonnichsen, T. Franzl, T. Wilk, G. Von Plessen, J. Feldmann, O. Wilson, P. Mulvaney, *Phys Rev Lett*, 2002, **88**, 7, 077402
31 S. Berciaud, L. Cognet, P. Tamarat, B. Lounis, *Nano Lett*, 2005, **5**, 3, 515-518
32 P.B. Johnson, R.W. Christy, *Phys. Rev. B*, 1972, **6**, 12, 4370
33 J. Bosbach, C. Hendrich, F. Stietz, T. Vartanyan, F. Trager, *Phys Rev Lett*, 2002, **89**, 25, 257404
34 T. Klar, M. Perner, S. Grosse, G. Von Plessen, W. Spirkl, J. Feldmann, *Phys Rev Lett*, 1998, **80**, 4249–4252
35 E. Prodan, C. Radloff, N.J. Halas, P. Nordlander, *Science*, 2003, **302**, 5644, 419-422
36 L.A. Peyser, A.E. Vinson, A.P. Bartko, R.M. Dickson, *Science*, 2001, **291**, 5501, 103-106
37 J. Zheng, R.M. Dickson, *J Am Chem Soc*, 2002, **124**, 47, 13982-13983
38 W.P. Wuelfing, S.M. Gross, D.T. Miles, R.W. Murray, *J Am Chem Soc*, 1998, **120**, 48, 12696-12697
39 G.A. Blab, L. Cognet, S. Berciaud, I. Alexandre, D. Husar, J. Remacle, B. Lounis, *Biophys J*, 2006, **90**, 1, L13-15
40 T.A. Taton, C.A. Mirkin, R.L. Letsinger, *Science*, 2000, **289**, 5485, 1757-1760
41 I. Alexandre, S. Hamels, S. Dufour, J. Collet, N. Zammatteo, F. De Longueville, J.L. Gala, J. Remacle, *Anal Biochem*, 2001, **295**, 1, 1-8
42 W. Fritzsche, T.A. Taton, *Nanotechnology*, 2003, **14**, 12, R63-R73
43 S.J. Park, T.A. Taton, C.A. Mirkin, *Science*, 2002, **295**, 5559, 1503-1506
44 R. Möller, R.D. Powell, J.F. Hainfeld, W. Fritzsche, *Nano Letters*, 2005, **5**, 7, 1475-1482
45 N. Zammatteo, S. Hamels, F. De Longueville, I. Alexandre, J.L. Gala, F. Brasseur, J. Remacle, *Biotechnol Annu Rev*, 2002, **8**, 85-101
46 C. Sonnichsen, B.M. Reinhard, J. Liphardt, A.P. Alivisatos, *Nat Biotechnol*, 2005, **23**, 6, 741-745
47 M.P. Sheetz, S. Turney, H. Qian, E.L. Elson, *Nature*, 1989, **340**, 6231, 284-288
48 K. Ritchie, X.Y. Shan, J. Kondo, K. Iwasawa, T. Fujiwara, A. Kusumi, *Biophys J*, 2005, **88**, 3, 2266-2277
49 A. Kusumi, Y. Sako, *Curr Opin Cell Biol*, 1996, **8**, 4, 566-574
50 A.J. Borgdorff, D. Choquet, *Nature*, 2002, **417**, 6889, 649-653
51 L. Cognet, L. Groc, B. Lounis, D. Choquet, *Science's STKE*, 2006, **2006**, 327
52 L. Cognet, C. Tardin, D. Boyer, D. Choquet, P. Tamarat, B. Lounis, *Proc Natl Acad Sci USA*, 2003, **100**, 20, 11350-11355